ELSEVIER

Tectonophysics 294 (1998) 333–347

TECTONOPHYSICS

Tides and tidal energetics of the Strait of Gibraltar: a modelling approach

Luis Tejedor [a,*], Alfredo Izquierdo [a], Dmitri V. Sein [b], Boris A. Kagan [b]

[a] *Departamento de Fisica Aplicada, Universidad de Cadiz, Cadiz, Spain*
[b] *Shirshov Institute of Oceanology, St. Petersburg Branch, Russian Academy of Sciences, St. Petersburg, Russia*

Received 15 May 1997; revised version received 3 November 1997; accepted 20 November 1997

Abstract

The main semidiurnal (M2 and S2) and diurnal (O1 and K1) tidal waves in the Strait of Gibraltar are simulated by employing a 2D high-resolution, non-linear, boundary-fitted coordinate model. Agreement between observational evidence and model results is good for the M2 and S2 tidal waves and satisfactory for the O1 and K1 tidal waves. The model reproduces all the known features of the spatial structure of these waves and predicts some new ones, namely, the general direction of the M2 and S2 mean tidal energy fluxes to the west, with a clear increase at the Camarinal Sill; the O1 amphidrome with anticlockwise rotation of cotidal lines in the Tarifa Narrows; and small-scale eddies in the M2, S2 and O1 mean tidal energy flux fields in the vicinity of the western and eastern boundaries of the Strait.

Keywords: surface tides; tidal energetics; numerical modelling; Strait of Gibraltar

1. Introduction

The Strait of Gibraltar has been the object of numerous tidal investigations. Suffice it to say that there are no less than nine tide gauge stations operating permanently along its coast. Two extensive surveys have been carried out in the Strait between 1960 and 1967 (Lacombe and Richez, 1982), and from Oct. 1985 to Oct. 1986 (Candela, 1990; Candela et al., 1990). The last campaign included bottom pressure and current velocity measurements at various locations within the Strait. Furthermore, at least three hydrodynamic tidal models of the Strait of Gibraltar have been developed by Sánchez and Pascual (1988), Wang (1989, 1993) and González et al. (1995). Hence, there exists a considerable amount of data for this rather small region which suggests that the qualitative and quantitative features of its tidal regime are now adequately understood. This, however, is not the case. Indeed, even those apparently obvious contradictions between the conclusions which were derived from the analysis of experimental data and the basic principles of tidal dynamics, as well as contradictions between model results and observational evidence, remain unexplainable.

The question arises of how to interpret an observed decrease in amplitude of the M2 tidal wave from the Atlantic to the Mediterranean Sea and a concurrent southwestern M2 phase propagation in

* Corresponding author. Tel./Fax: +34 956 470 866; E-mail: luis.tejedor@uca.es

0040-1951/98/$19.00
PII: S0040-1951(98)00110-3

the Strait of Gibraltar (Candela, 1990; Candela et al., 1990)? How is this phase propagation compatible with a substantial tidal energy transport from the Strait to the Mediterranean Sea, which was adopted in the model of Wang (1989, 1993) for the Strait of Gibraltar and in the models of Tsimplis et al. (1995) and Lozano and Candela (1995) for the Mediterranean Sea? Why is a two-fold decrease in the M2 amplitude in the Strait of Gibraltar accompanied by small variations in phase and an almost 90º-phase difference between tidal velocity and tidal elevation? Why do the amplitude ratios and phase differences between the O1 and K1 tidal waves vary greatly throughout the Strait, in contrast to the M2 and S2 tidal waves? Are these phase differences a consequence of the existence of an elevation node in the Strait, as speculated García (1986), and, if so, is this node transformed into an amphidrome? These questions as well as the necessity to provide precise quantitative estimates of tidal loading which are required for geodetic applications stimulated this work.

The present paper is organised as follows: we first give a brief description of the hydrodynamic model employed. In Section 3, we then present the validation of simulation results and discuss the spatial structure of the tidal characteristics corresponding to the M2, S2, O1 and K1 tidal waves. Tidal energetics are dealt with in Section 4 and the sensitivity of model results to boundary forcing is discussed in Section 5. Conclusions are drawn in Section 6.

2. Model description

The model used for simulating the semidiurnal and diurnal tides in the Strait of Gibraltar is a 2D high-resolution, non-linear, boundary-fitted coordinate model. A detailed description of this model is given in Tejedor et al. (1997). A free-slip condition for velocity in the contravariant variables is applied to the coastal boundaries. At the open boundaries, the tidal elevation is prescribed as a periodic function of time. The depth-averaged tidal dynamics equations in a boundary-fitted coordinate system are integrated on the Arakawa C staggered grid employing the splitting method and the semi-implicit Crank–Nicolson scheme.

The curvilinear grid with a nominal spatial resolution of 0.5 km is displayed in Fig. 1, together with a bathymetric chart of the domain under study. The tidal constants at the open boundary grid nodes are found by interpolation from those measured at the coastal stations *Trafalgar* and *Espartel* on the western end and the coastal stations *Gibraltar* and *Ceuta* on the eastern end of the Strait. In order to minimise the errors obtained when evaluating the O1 and K1 phases at the western boundary where large variations are observable, the coastal stations *Trafalgar* and *Espartel* are supplemented with the deep water bottom pressure station DW. The bathymetry is derived from Admiralty Navigation Charts. The time step was taken to be 20 s. The model is run for 25 days to achieve a stable, time-periodic solution. After establishing the time-periodic regime, the model run was continued for a 29-day period; thereafter a harmonic analysis is performed on the tidal elevation and velocity so that the cotidal charts and the charts of tidal current parameters can be constructed.

3. Tides and tidal currents

The calculated cotidal charts for the M2, S2, O1 and K1 tidal waves are shown in Figs. 2–5. The first two figures compare favourably with the results of Candela et al. (1990) which were derived from analysis of tide gauge and bottom pressure observations. In particular, these charts show a more than two-fold reduction in the M2 amplitudes between the western and eastern ends of the Strait, as well as their invariability in the across-strait direction, a small change in the M2 phases along the Strait with a clear propagation southwestward, and also fairly constant amplitude ratios and phase differences between the M2 and S2 constituents throughout the Strait. By way of illustration, we notice that the above amplitude ratios and phase differences vary within the Strait from 2.45 to 2.55 and -23.5^{o} to -28.0^{o}, respectively.

The most remarkable feature of the cotidal chart for the O1 tidal wave is an amphidrome in the Tarifa Narrows, with anticlockwise rotation of cotidal lines and its centre displaced northward from the Strait's axis. Its origin is due to the existence of antiphase oscillations in the adjacent regions of the North At-

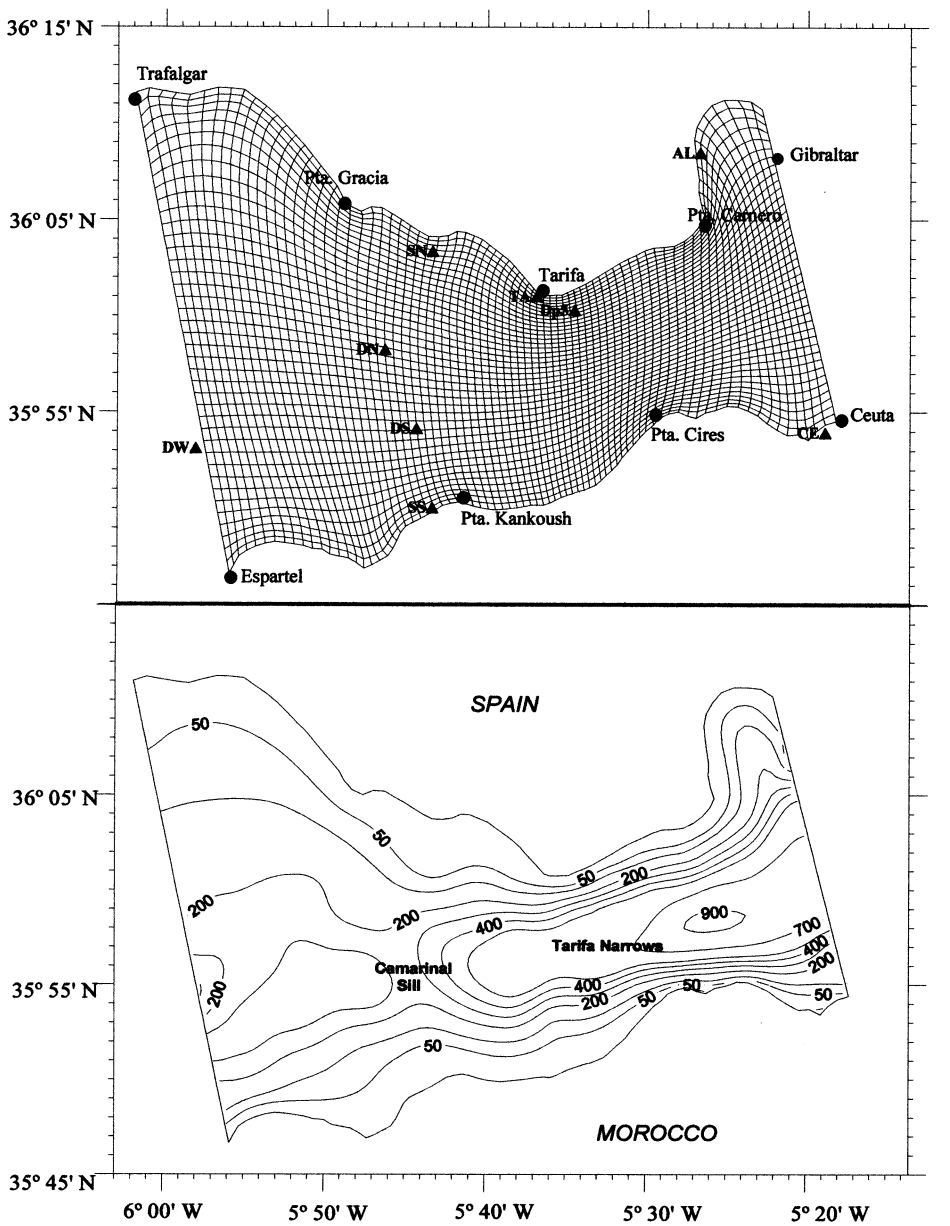

Fig. 1. Grid map of the Strait of Gibraltar. Also shown are the locations of the tide gauge (solid circles) and bottom pressure (solid triangles) measurement sites referred to in the text (upper), as well as the bathymetric chart of the Strait of Gibraltar (lower).

lantic and the Mediterranean Sea. Unlike the O1, the K1 tidal wave with a near-quadrature phase difference between both ends of the Strait does not form an amphidrome. This wave resembles a mixed, progressive-standing wave marked by a veering of cotidal lines and an increase in amplitudes when moving away from the northern coast. Hence, the existence of the O1 amphidrome and major differences between the O1 and K1 tides should be attributable to different external forcings at both ends of the Strait. The above features in the spatial structure of the O1 and K1 surface tides, which are governed by

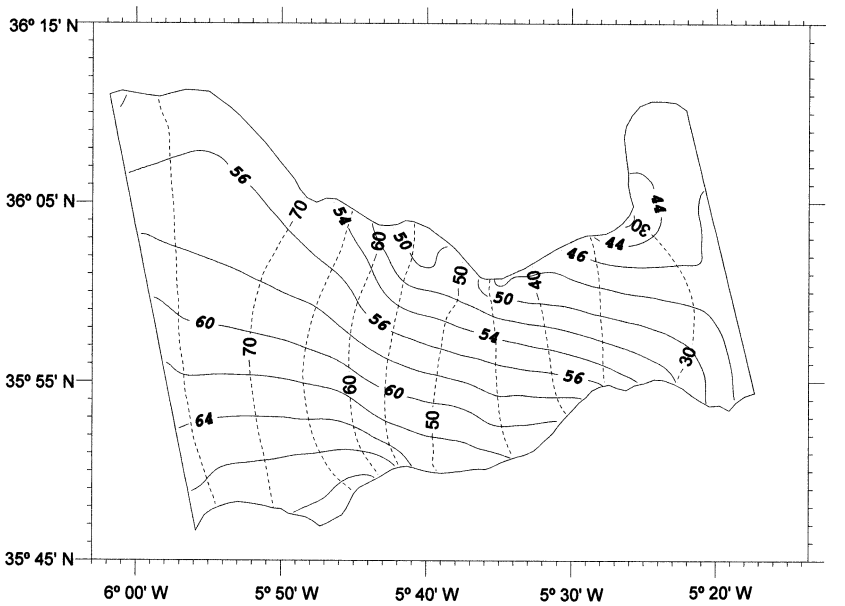

Fig. 2. Cotidal chart of the M2 tidal wave. Solid lines are phase contours (deg), dashed lines are amplitudes (cm).

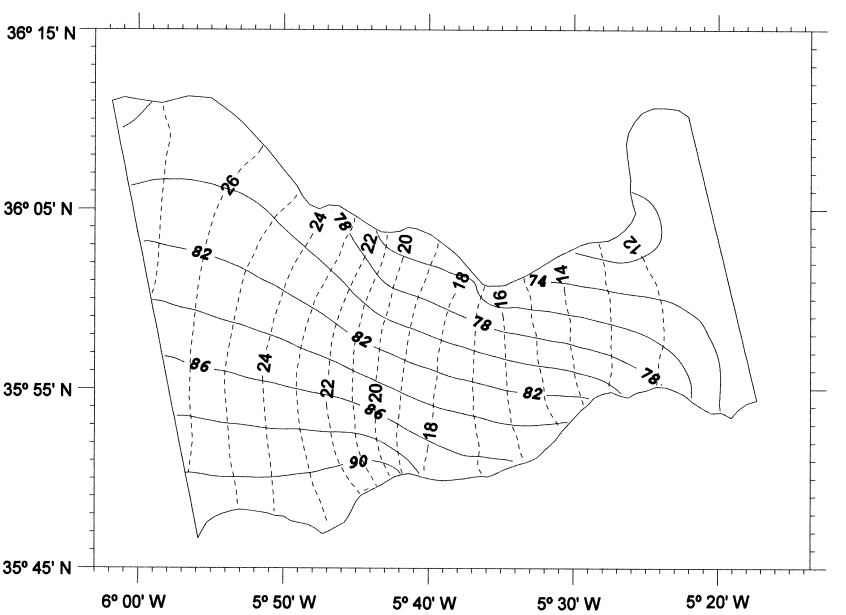

Fig. 3. The same as in Fig. 2, but for the S2 tidal wave.

different boundary forcings at both ends of the Strait, explain the variations in the amplitude ratios and phase differences between the major diurnal tidal constituents mentioned in Section 1.

A comparison of predicted tidal constants with observational data at coastal tide gauge and bottom pressure stations is presented in Tables 1 and 2. As can be seen, the maximum differences do not exceed 7.0 cm (that is, about 10% in relative units) for the M2 and S2 amplitudes and 10º for their phases. Agreement between observed and predicted tidal constants for the O1 and K1 tidal waves is,

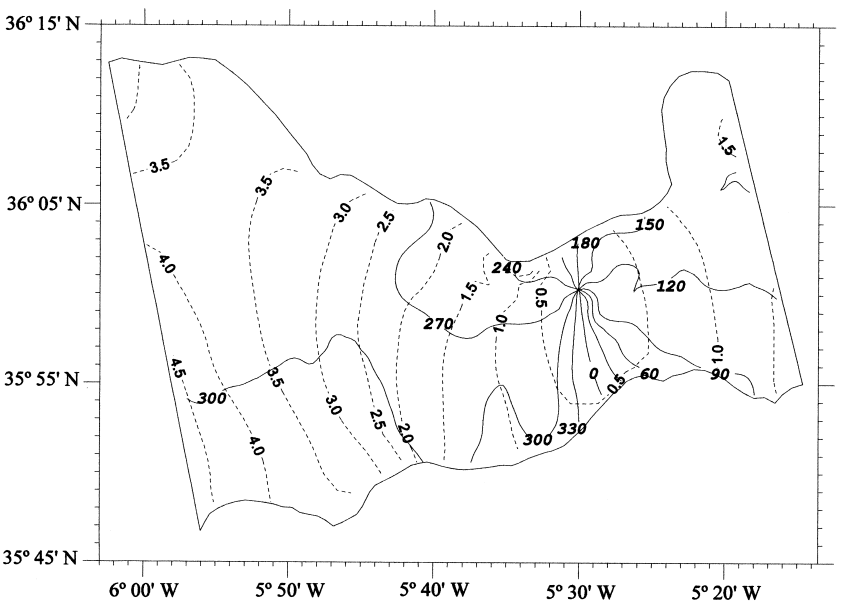

Fig. 4. The same as in Fig. 2, but for the O1 tidal wave.

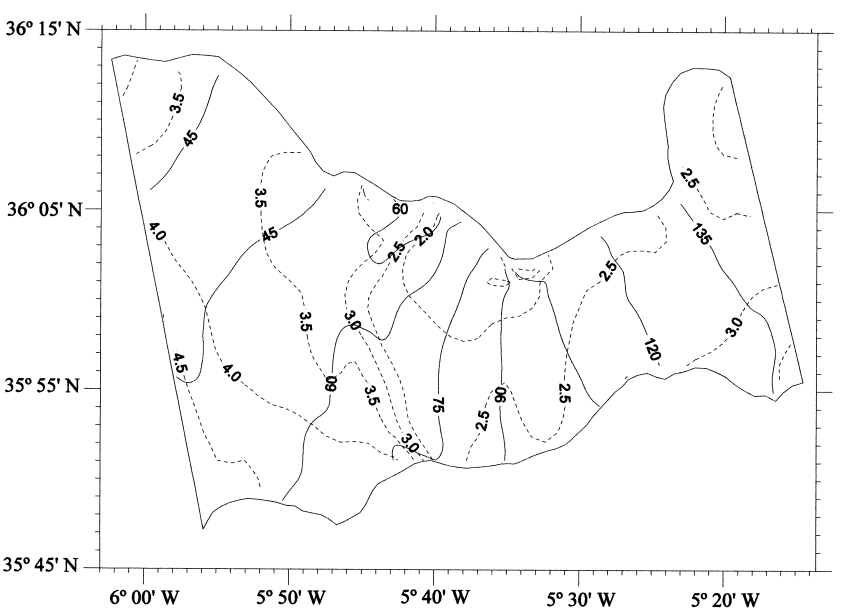

Fig. 5. The same as in Fig. 2, but for the K1 tidal wave.

in general, satisfactory but worse than for the M2 and S2 tidal waves. This is because, first, the spatial resolution employed appears to be insufficient to resolve some local features of bathymetry and coast line configuration; second, the diurnal tides are very sensitive to small variations in morphometry due to their small amplitudes; third, the estimates of tidal constants for the O1 and K1 tides derived from bottom pressure measurements via harmonic analysis or admittance calculations are not without faults since, according to Candela et al. (1990), the energy content in the diurnal spectral band is within

Table 1
A comparison of modeled amplitudes (A) and phases (g) with data of tide gauges and bottom pressure measurements

Site	Latitude North	Longitude West	M2				S2			
			Observed		Predicted		Observed		Predicted	
			A (cm)	g (deg)	A (cm)	g (deg)	A (cm)	g (deg)	A (cm)	g (deg)
Pla. Gracia	36º05.4′	05º48.6′	64.9 ± 0.2	49 ± 0.5	70.4	55.0	22.3 ± 0.2	74.0 ± 1.0	24.7	78.8
DN	35º58′	05º46′	60.1	51.8	61.6	58.1	22.5	73.8	21.6	82.3
DS	35º54′	05º44′	54.0	61.8	57.4	61.2	21.1	83.3	20.2	85.8
SN	36º03′	05º43′	52.3	47.6	59.3	51.4	18.5	73.4	21.0	75.9
SS	35º50′	05º43′	57.1	66.8	58.9	67.3	20.6	92.3	20.4	91.4
DW	35º53′	05º58′	78.5	56.1	76.1	63.6	29.0	82.2	26.3	88.2
Kankoush	35º50.5′	05º41.0′	51.8 ± 0.4	69 ± 0.5	52.4	63.7	20.1 ± 0.4	90.0 ± 2.0	18.3	88.2
Tarifa	36º00.2′	05º36.4′	41.5 ± 0.2	57 ± 0.5	47.4	49.9	14.2 ± 0.2	85.0 ± 1.0	17.1	75.8
TA	36º01′	05º36′	41.2	41.2	45.8	49.8	14.7	67.9	16.6	75.8
Dp5	36º00′	05º34′	44.4	47.6	42.2	49.2	16.1	73.9	15.5	75.4
Pta. Cires	35º54.7′	05º28.8′	36.4 ± 0.2	46.5 ± 0.5	36.7	56.8	14.1 ± 0.2	74.0 ± 1.0	13.7	81.6
AL	36º08′	05º26′	31.0	48.0	27.5	44.5	11.1	73.9	11.0	72.7
Pta. Carnero	36º04.3′	05º25.7′	31.1 ± 0.2	47.5 ± 0.5	29.3	42.0	11.5 ± 0.2	71.0 ± 1.0	11.5	70.8
CE	35º53′	05º18′	29.7	50.3	29.3	48.2	11.4	75.6	11.1	73.1

Sources are as follows: García (1986) and Candela et al. (1990); here ± indicates standard errors.

Table 2
A comparison of modeled amplitudes (A) and phases (g) with data of tide gauges and bottom pressure measurements

Site	Latitude North	Longitude West	K1				O1			
			Observed		Predicted		Observed		Predicted	
			A (cm)	g (deg)	A (cm)	g (deg)	A (cm)	g (deg)	A (cm)	g (deg)
Pta. Gracia	36º05.4′	05º48.6′	3.7 ± 0.2	75 ± 4	3.4	39.6	1.8 ± 0.2	313 ± 8	3.4	282.8
DN	35º58′	05º46′	2.5	83.3	2.8	56.6	1.5	291.7	2.5	286.8
DS	35º54′	05º44′	4.4	76.3	3.0	68.6	2.8	335.7	2.2	299.6
SN	36º03′	05º43′	2.1	95.3	2.7	63.8	0.7	298.0	2.2	288.2
SS	35º50′	05º43′	5.3	68.6	4.0	76.9	3.8	332.0	2.7	327.4
Kankoush	35º50.5′	05º41.0′	4.6 ± 0.4	88 ± 5	2.3	73.9	2.9 ± 0.4	343 ± 8	1.7	281.0
Tarifa	36º00.2′	05º36.4′	2.2 ± 0.2	131 ± 5	1.8	92.7	0.5 ± 0.2	165 ± 25	1.3	266.1
TA	36º01′	05º36′	2.1	145.5	1.7	94.5	1.2	104.7	1.3	257.5
Dp5	36º00′	05º34′	0.8	92.2	1.83	108.2	1.7	225.3	0.7	234.6
Pta. Cires	35º54.7′	5º28.8′	3.2 ± 0.2	133 ± 4	3.0	111.9	1.2 ± 0.2	81 ± 10	0.6	34.1
AL	36º08′	05º26′	2.1	147.6	2.5	145.5	1.1	106.9	1.5	147.8
Pta. Carnero	36º04.3′	05º25.7′	2.3 ± 0.2	145 ± 5	2.9	136.3	0.7 ± 0.2	181 ± 17	1.2	121.5
CE	35º53′	05º18′	3.6	143.4	3.3	135.3	2.0	102.7	1.6	99.8

Sources are as follows: García (1986) and Candela et al. (1990); here ± indicates standard errors.

the noise limits produced by internal tidal waves; and, finally, various sources often contain different values for tidal constants, especially for phases.

The calculated fields of major and minor axes of the M2 and S2 tidal current ellipses are shown together with their sense of rotation in Figs. 6 and 7. The first point to note is the almost rectilinear nature of the semidiurnal tidal current in most parts of the Strait, exceptions being the northwestern and eastern regions adjacent to the open boundaries. Extreme values of maximum current velocity (100–110 cm/s for M2 and 25–30 cm/s for S2) are predicted at the Camarinal Sill. To the west and east of the sill and in the Tarifa Narrows they do not exceed 70 cm/s

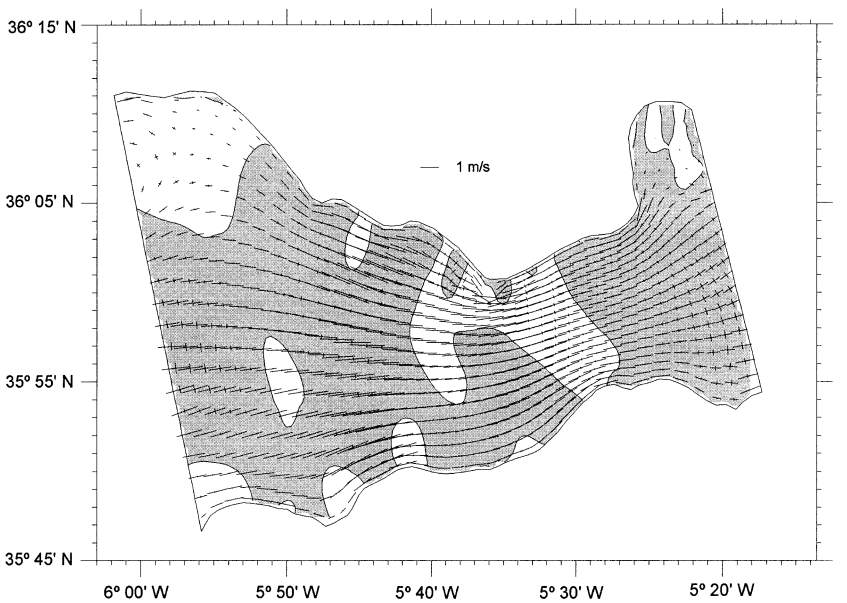

Fig. 6. Major and minor axes of the tidal ellipses and sense of rotation of the current velocities for the M2 tidal wave. Velocity scale is indicated at the top of the figure; shaded and unshaded regions correspond to clockwise and anticlockwise rotation, respectively.

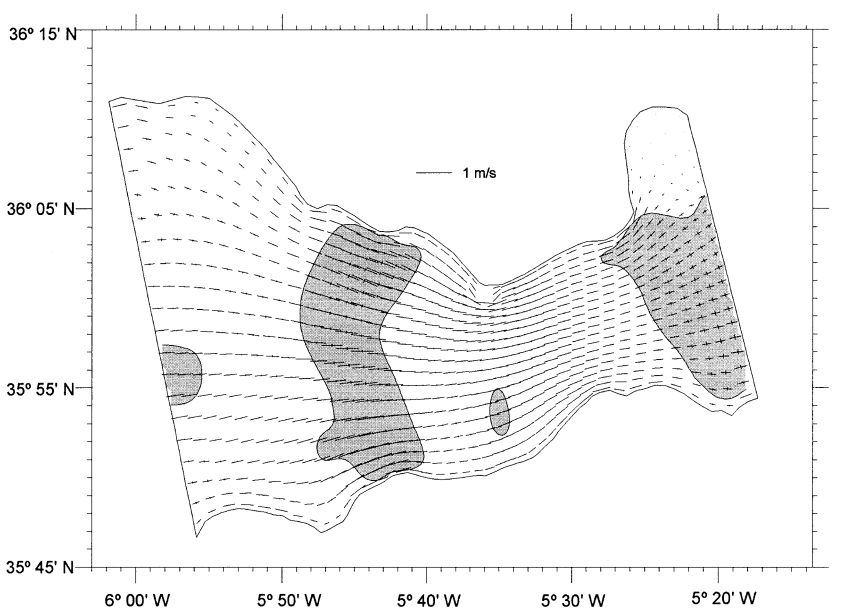

Fig. 7. The same as in Fig. 6, but for the S2 tidal wave.

for the M2 tidal current and 20 cm/s for the S2 tidal current.

The most important feature of the M2 and S2 tidal currents in the Strait of Gibraltar is the phase difference between maximum current velocity and tidal elevation. As can be seen, it is ∼90º everywhere except for the northwestern and eastern regions (Figs. 10 and 11). This feature can be due to topographic funnelling which, in a weakly dissipative convergent channel having a topographic

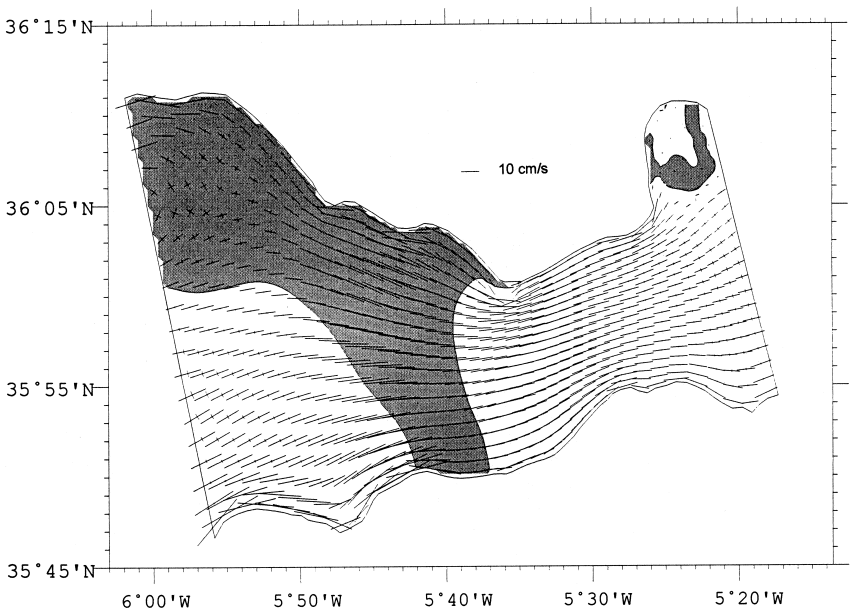

Fig. 8. The same as in Fig. 6, but for the O1 tidal wave.

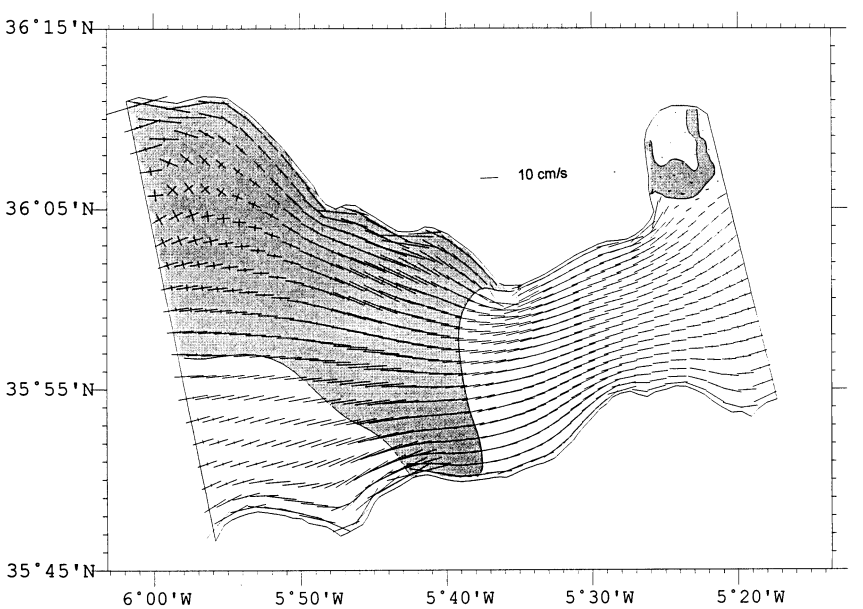

Fig. 9. The same as in Fig. 6, but for the K1 tidal wave.

length scale much smaller than the characteristic tidal wavelength, is responsible for the transformation of a progressive wave into a standing wave (Jay, 1991; Tejedor et al., 1997).

The calculated fields of major and minor axes of the O1 and K1 tidal current ellipses are outlined in Figs. 8 and 9. The O1 tidal currents are weak (i.e. <10 cm/s) in most parts of the Strait. An exception is the region off the southern coast between Tangier and Pta. Altares where maximum velocities can be as large as 16 cm/s. Similar features are exhibited by the K1 tidal currents, however the region where

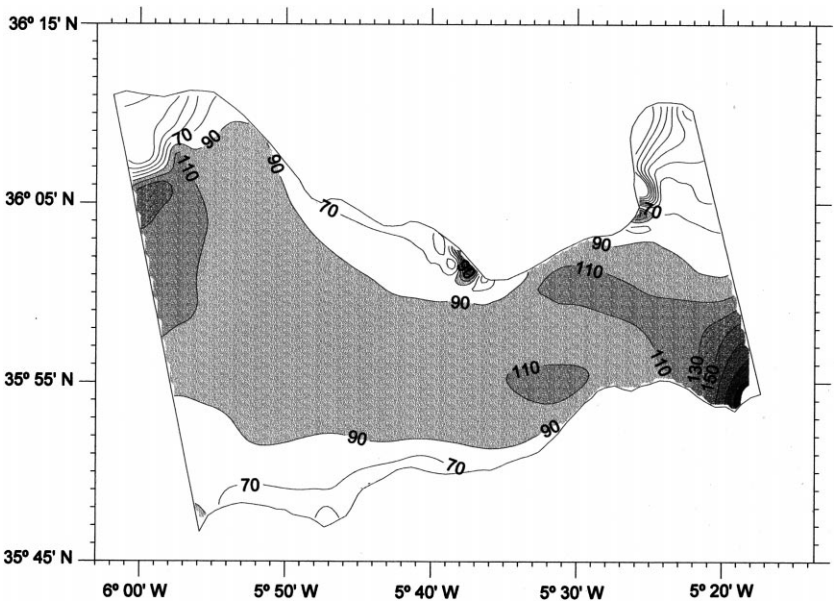

Fig. 10. Phase difference, in degrees, between maximum tidal current velocity and tidal elevation for the M2 tidal wave.

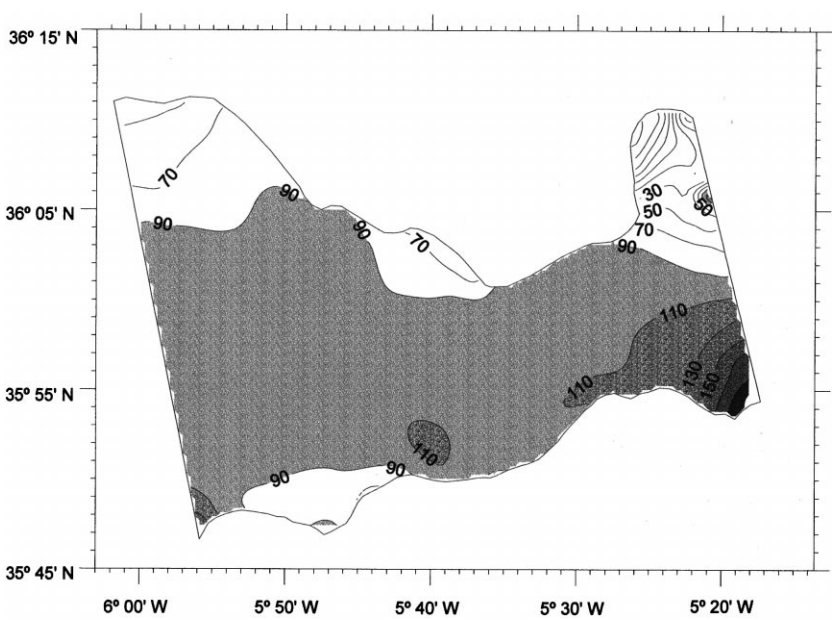

Fig. 11. The same as in Fig. 10, but for the S2 tidal wave.

maximum velocities reach 16 cm/s is now located close to the northern coast between C. Trafalgar and Pta. Paloma. Apart from the northwestern region of the Strait, the O1 and K1 tidal currents are almost rectilinear and have an along-coast orientation in the offshore region and an along-strait orientation in the central part of the Strait. The maximum offshore current velocities exceeding 10–14 cm/s are found solely at the Camarinal Sill and are only half this value in the Tarifa Narrows due to increasing depth.

As stated in Tejedor et al. (1997), a good quantitative agreement between observed and predicted values of the semidiurnal tidal current ellipse parameters is obtained. Comparison of predicted values of the diurnal tidal current parameters with observational data is, however, impossible because of the inherent uncertainties in determining the diurnal tidal currents from current meter measurements.

4. Tidal energetics

In such a small basin like the Strait of Gibraltar, which has dimensions being much less than the length scale of the tide-generating force, the tidal cycle-averaged energy budget is mainly determined by the divergence of the mean tidal energy flux and the mean rate of tidal energy dissipation. In other words, the resulting difference between the mean tidal energy fluxes into and out of the Strait must be balanced by the tidal dissipation within the Strait.

The spatial distributions of the M2 and S2 mean tidal energy fluxes (see Figs. 12 and 13) indicate that in most parts of the Strait these fluxes are relatively small. This is the result of the phase difference between maximum current velocity and sea level tidal elevation being nearly 90º. The maximum (by magnitude) mean tidal energy flux per unit length are -3.4×10^5 W/m for M2 and -0.42×10^5 W/m for S2 (hereinafter, minus sign indicates westward direction of the flux). These values occur only in the vicinity of the eastern boundary of the Strait. At the Camarinal Sill and in the central part of the Tarifa Narrows, the mean tidal energy fluxes are less than -2.8×10^5 W/m for M2 and -0.28×10^5 W/m for S2. The net (i.e. cross-section integrated) mean tidal energy fluxes through the eastern and the western boundaries are, respectively, -20.2×10^8 W and -14.7×10^8 W for M2 and -2.3×10^8 W and -2.1×10^8 W for S2.

As can be seen from Figs. 12 and 13, the M2 and S2 mean tidal energy fluxes are changing in the cross-strait direction such that their values are decreasing when approaching the coast. Accordingly, any local estimates of the mean tidal energy flux obtained at any point and then extended to the entire Strait's cross section should be used with reservation. From these figures it also follows that the general direction of the M2 and S2 mean tidal energy fluxes is to the west over much of the Strait, exception being the vicinity of the eastern and western boundaries where small-scale eddy structures occur. This result conforming to the southwestern phase propagation of the M2 and S2 surface tides (Candela, 1990; Candela et al., 1990; García, 1986) points to the need

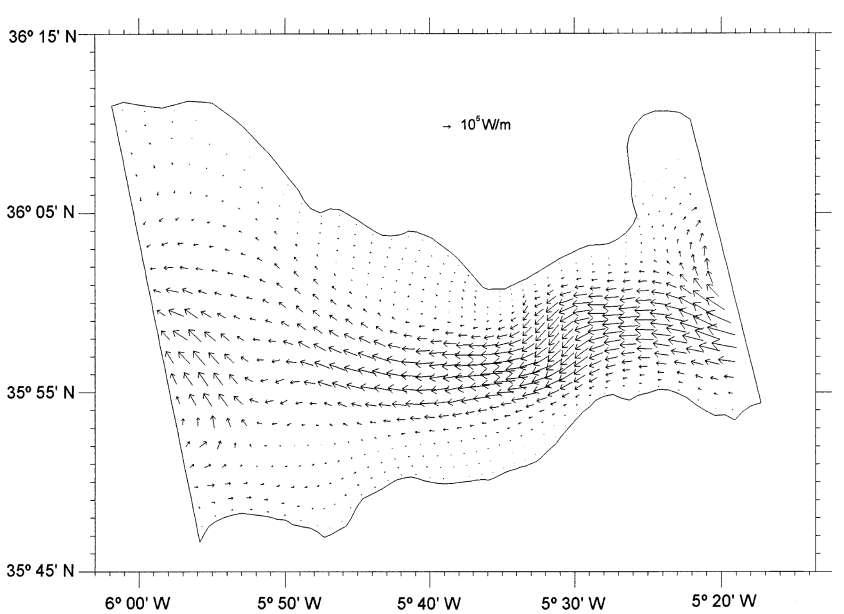

Fig. 12. Mean tidal energy flux for the M2 tidal wave. Flux scale (10^5 W/m) is indicated at the top of the figure.

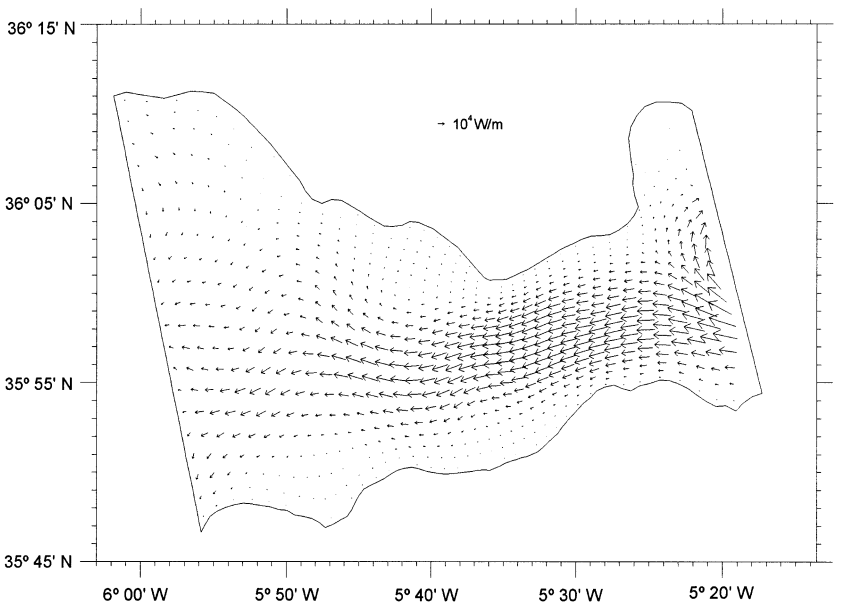

Fig. 13. The same as in Fig. 12, but for the S2 tidal wave. Flux scale is 10^4 W/m.

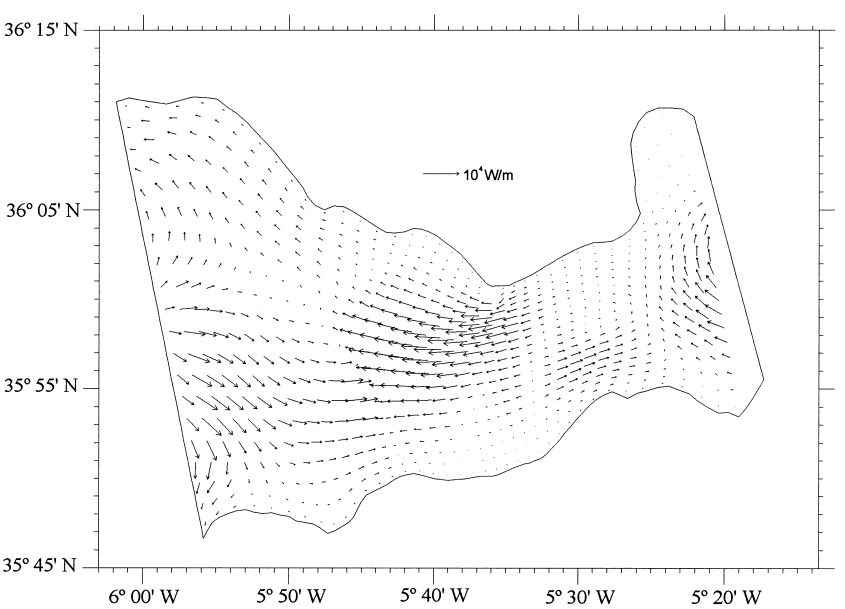

Fig. 14. The same as in Fig. 12, but for the O1 tidal wave. Flux scale is 10^4 W/m.

for revision of the traditional view of the Strait of Gibraltar as a carrier of tidal energy from the North Atlantic to the Mediterranean Sea.

A distinctly different situation occurs for the O1 and K1 mean tidal energy fluxes. As is evident from Fig. 14, the O1 tidal wave is characterised by the lack of general directionality in the mean tidal energy flux within the Strait. The most important features of the pattern obtained are, first, the appearance of an anticlockwise gyre in the vicinity of the amphidrome

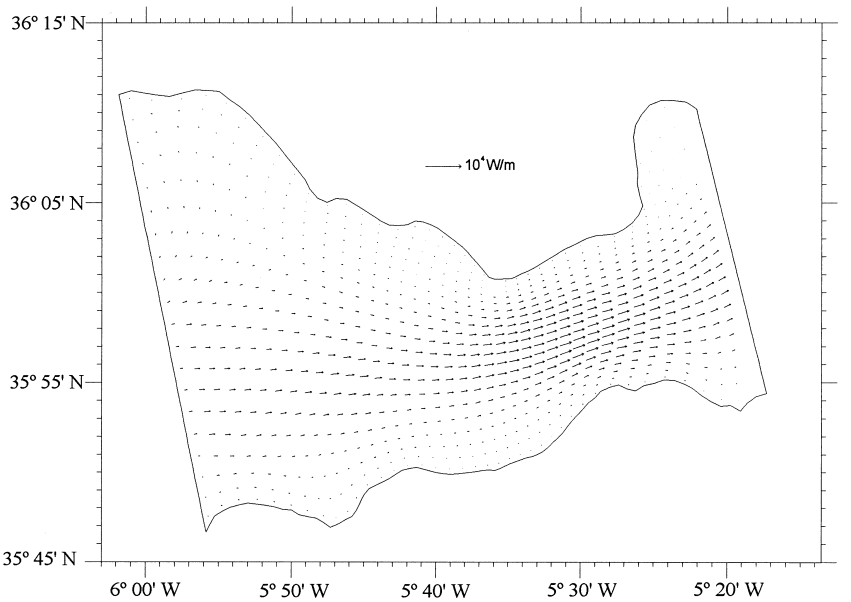

Fig. 15. The same as in Fig. 12, but for the K1 tidal wave. Flux scale is 10^4 W/m.

centre; second, an intensification of the fluxes on the eastern slope of the Camarinal Sill, with the general tendency for them to drive energy to the west; and, third, generation of a system of one clockwise eddy and one anticlockwise eddy in the western part and a clockwise eddy in the eastern part of the Strait. In contrast (see Fig. 15), the general direction of the K1 mean tidal energy flux is to the eastnortheast, with a clear intensification in the Tarifa Narrows and no accompanying eddies developing in the Strait. The net tidal energy fluxes through the western and the eastern boundaries are, respectively, 0.109×10^8 W and 0.018×10^8 W for O1 and 0.540×10^8 W and 0.468×10^8 W for K1, indicating thereby that the bulk of the O1 tidal energy dissipates within the Strait and that, unlike the M2 and S2, the O1 and K1 net tidal energy fluxes are directed eastward

Figs. 16–19 depict the spatial distributions of mean tidal energy dissipation due to bottom friction for the M2, S2, O1 and K1 tidal waves. As expected, the tidal energy dissipation at the Camarinal Sill greatly exceeds those predicted in other parts of the Strait. Considering that this strong local sink of tidal energy occupies a sizeable area of the Strait, it is not surprising that it controls the total tidal energy dissipation. The latter is estimated to be 5.5×10^8 W for the M2 tidal wave, 0.2×10^8 W for the S2 tidal wave, 0.9×10^7 W for the O1 tidal wave and 0.72×10^7 W for the K1 tidal wave.

We have already mentioned the existence of small-scale eddies in the mean tidal energy flux fields near the eastern and western boundaries. The fact that these eddies are present in the M2, S2 and O1 mean tidal energy flux fields and absent in the K1 mean tidal energy flux fields indicates convincingly that these owe their origin to both end and topographic funnelling effects.

5. Sensitivity to boundary forcing

In order to evaluate how robust the results obtained are there is a need to vary boundary forcing. For this purpose the tidal constants at the western boundary grid nodes were set by employing a linear, piece-wise interpolation of the observed values at tide gauge stations Trafalgar and Espartel and bottom pressure station DW, rather than of the first two of them only, for M2 and S2 and a parabolic interpolation, instead of a linear one, for O1 and K1. All the other conditions of the experiment were retained with no modifications.

The resulting solutions for the M2, S2, K1 and O1 surface tides are identical in a qualitative sense to

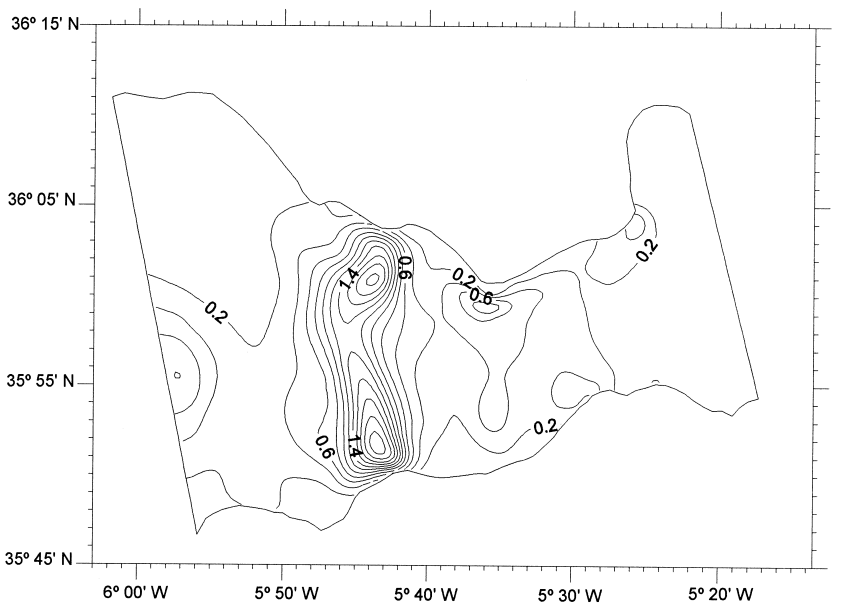

Fig. 16. Tidal energy dissipation (W/m^2) for the M2 tidal wave.

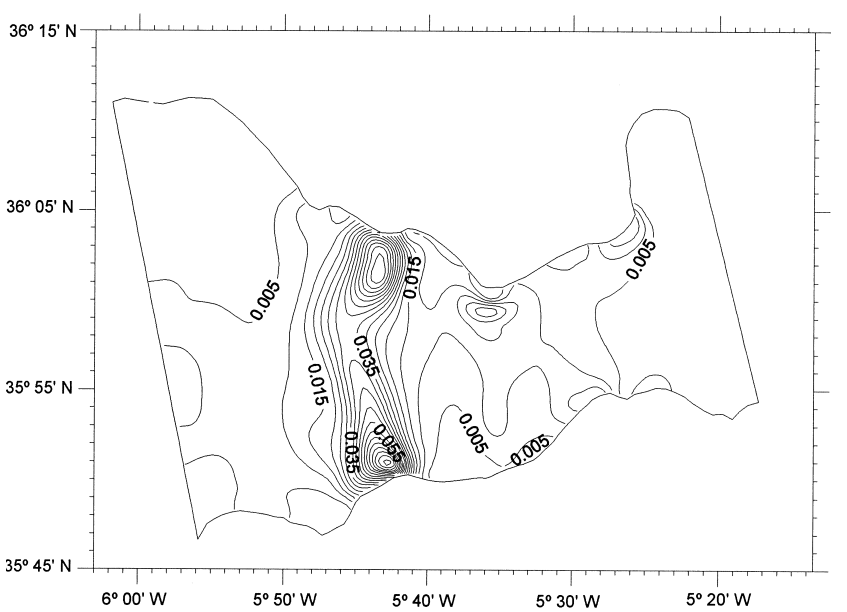

Fig. 17. The same as in Fig. 16, but for the S2 tidal wave.

those displayed in Figs. 2–19. As expected, the quantitative changes of tidal characteristics are mainly concentrated in the western part of the Strait. But even there they are modest and do not essentially affect the general direction of the M2 and S2 mean tidal energy fluxes westward and the position of the O1 amphidrome in the Tarifa Narrows. Also, the rms differences between predicted and observed tidal elevation amplitudes and phases obtained by the two methods for specifying the tidal constants at the western boundary grid nodes are in close agreement. The minimum rms differences therewith occur when

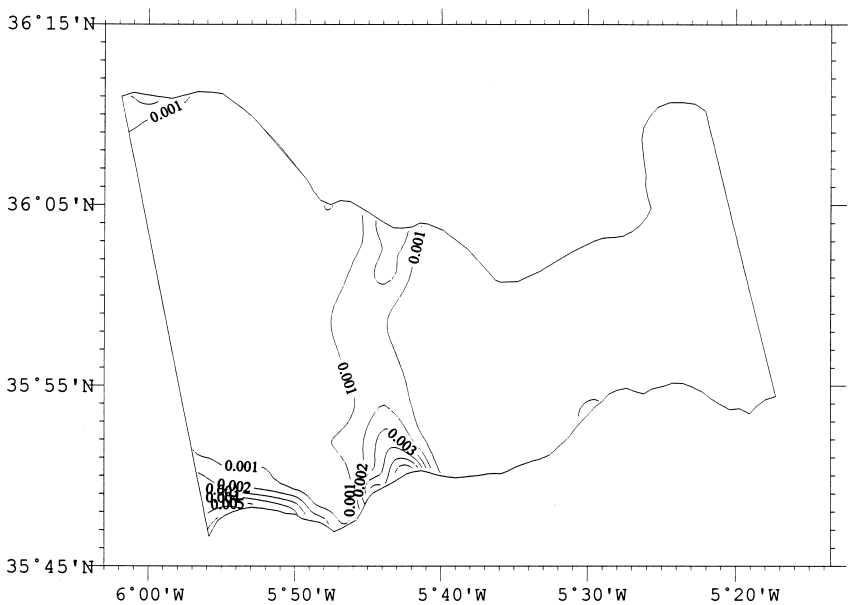

Fig. 18. The same as in Fig. 16, but for the O1 tidal wave.

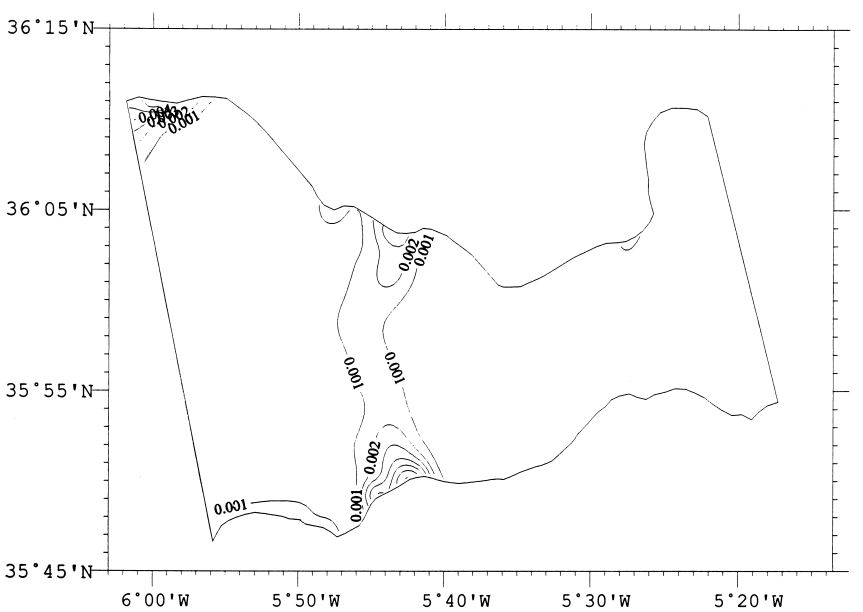

Fig. 19. The same as in Fig. 16, but for the K1 tidal wave.

using the two-point linear interpolation for M2 and S2 and the three-point linear interpolation for K1 and O1. By the way, that is why these interpolation procedures were chosen to run the model in the control case (Sections 3 and 4).

6. Conclusion

A 2D high-resolution, non-linear, boundary-fitted coordinate model has been applied for simulating the semidiurnal (M2 and S2) and diurnal (O1 and

K1) tides in the Strait of Gibraltar. The predicted tidal constants are in good agreement with those derived from coastal tide gauge and bottom pressure measurements. The model reproduces all the known features of the spatial structure of the tides under consideration and predicts some new ones as well. These new features are the O1 amphidrome with anticlockwise rotation of cotidal lines in the Tarifa Narrows, the general direction of the M2 and S2 mean tidal energy fluxes to the west, with a clear increase in the vicinity of the Camarinal Sill, the existence of small-scale eddies in the M2, S2 and O1 mean tidal energy flux fields near the open boundaries of the Strait, and the lack of such eddies in the K1 mean tidal energy flux field.

The presence of small-scale eddies adjacent to the open boundaries predetermines the decrease of O1 mean tidal energy transport through the Strait. This fact, as well as and especially the fact that the general direction of the M2 and S2 mean tidal energy transports is to the west, not only eliminate the contradiction between the observed southwestern phase propagation and a commonly used mean tidal energy transport eastward, but can also change the traditional view of the Strait of Gibraltar as a carrier of tidal energy from the North Atlantic into the Mediterranean Sea.

The high-resolution tidal maps presented here may have applications in oceanic tidal loading computations which are enabling corrections for high precision gravity measurements and even GPS measurements in such a complex tectonic region as the Gibraltar Arc (Vieira et al., 1982, 1985).

Acknowledgements

This work was carried out during a stay of B.A. Kagan as visiting professor at University of Cadiz. The authors are greatly indebted to the reviewers for their constructive criticism of an earlier version of the manuscript. This work was supported by the EC Project SELF-II, under contract CT 95-0087 and by the INTAS Project No 96-1875.

References

Candela, J., 1990. The barotropic tide in the Strait of Gibraltar. In: Pratt, L.J. (Ed.), The Physical Oceanography of Sea Straits. Kluwer, Dordrecht, pp. 457–475.

Candela, J., Winant, C., Ruiz, A., 1990. Tides in the Strait of Gibraltar. J. Geophys. Res. 95, 7313–7335.

García Lafuente, J.M., 1986. Variabilidad del nivel del mar en el Estrecho de Gibraltar: Mareas y oscilaciones residuales, Ph.D Thesis, Instituto Español de Oceanografía, Fuengirola, Málaga, Spain, 154 pp.

González, M., García, M.A., Espino, M., Sánclez-Arcilla, A., 1995. Un modelo numérico en elementos finitos para la corriente inducida por la marea. Aplicaciones al Estrecho de Gibraltar. Rev. Int. Métodos Num. Calc. Diseño Ing. 11, 383–400.

Jay, D.A., 1991. Green's law revisited: Tidal long-wave propagation in channels with strong topography. J. Geophys. Res. 96, 20585–20598.

Lacombe, H., Richez, C., 1982. The regime of the Strait of Gibraltar. In: Nihoul, J.C.J. (Ed.), Hydrodynamics of Semi-enclosed Seas. Elsevier, Amsterdam, pp. 13–74.

Lozano, C.J., Candela, J., 1995. The M_2 tide in the Mediterranean Sea: Dynamical analysis and data assimilation. Oceanol. Acta 18, 419–441.

Sánchez, P., Pascual, J.R., 1988. Primeras experiencias en la modelación del Estrecho de Gibraltar. In: Almazán, J.L., Bryden, H.L., Kinder, T.H., Parrilla, G. (Eds.), Seminario Sobre la Oceanografía Física del Estrecho de Gibraltar. Escuela Superior Ing. Cammos, Canales y Puertos, Madrid, pp. 251–28.

Tejedor, L., Izquierdo, A., Kagan, B.A., Sein, D.V., 1997. Simulation of the semidiurnal tides in the Strait of Gibraltar. J. Geophys. Res. (submitted for publication).

Tsimplis, M.N., Proctor, R., Flather, R.A., 1995. A two-dimensional tidal model for the Mediterranean Sea. J. Geophys. Res. 100, 16223–16239.

Vieira, R., Toro, C., Sukhwani, P., 1982. Ocean effects on gravity tides in the Iberian Peninsula, Proc. IX Int. Symp. Earth Tides. E. Schweizerbat'she Verlag, pp. 431–436.

Vieira, R., Toro, C., Megias, E., 1985. Ocean tides in the nearby of the Iberian peninsula. Part 1: M2 Iberia Map, Proc. X Int. Symp. Earth Tides, C.S.I.C., Madrid, pp. 679–695.

Wang, D.P., 1989. Model of mean and tidal flows in the Strait of Gibraltar. Deep-Sea Res. 36, 1535–1548.

Wang, D.P., 1993. The Strait of Gibraltar model: internal tide, diurnal inequality and fortnightly modulation. Deep-Sea Res. 40, 1187–1203.